A selective chemical probe for exploring the role of CDK8 and CDK19 in human disease

Trevor Dale[1,4]*, Paul A Clarke[2,4]*, Christina Esdar[3], Dennis Waalboer[2], Olajumoke Adeniji-Popoola[2], Maria-Jesus Ortiz-Ruiz[2], Aurélie Mallinger[2], Rahul S Samant[2], Paul Czodrowski[3], Djordje Musil[3], Daniel Schwarz[3], Klaus Schneider[3], Mark Stubbs[2], Ken Ewan[1], Elizabeth Fraser[1], Robert TePoele[2], Will Court[2], Gary Box[2], Melanie Valenti[2], Alexis de Haven Brandon[2], Sharon Gowan[2], Felix Rohdich[3], Florence Raynaud[2], Richard Schneider[3], Oliver Poeschke[3], Andree Blaukat[3], Paul Workman[2], Kai Schiemann[3], Suzanne A Eccles[2], Dirk Wienke[3]* & Julian Blagg[2]*

There is unmet need for chemical tools to explore the role of the Mediator complex in human pathologies ranging from cancer to cardiovascular disease. Here we determine that CCT251545, a small-molecule inhibitor of the WNT pathway discovered through cell-based screening, is a potent and selective chemical probe for the human Mediator complex–associated protein kinases CDK8 and CDK19 with >100-fold selectivity over 291 other kinases. X-ray crystallography demonstrates a type 1 binding mode involving insertion of the CDK8 C terminus into the ligand binding site. In contrast to type II inhibitors of CDK8 and CDK19, CCT251545 displays potent cell-based activity. We show that CCT251545 and close analogs alter WNT pathway–regulated gene expression and other on-target effects of modulating CDK8 and CDK19, including expression of genes regulated by STAT1. Consistent with this, we find that phosphorylation of STAT1[SER727] is a biomarker of CDK8 kinase activity *in vitro* and *in vivo*. Finally, we demonstrate *in vivo* activity of CCT251545 in WNT-dependent tumors.

The discovery of chemical probes based on testing libraries of small molecules against cellular pathway screens has re-emerged as a credible hit-discovery strategy, particularly for signaling networks lacking well-validated druggable targets. The success of these approaches is highly dependent upon the quality of the cell-based assay cascade and the chemical library in order to minimize false-positive responses[1,2]. Subsequent hit-series optimization and proximal biomarker discovery are greatly facilitated by identification of the molecular targets, and this, in turn, requires the design and synthesis of appropriate chemical tools for target pulldown and cellular proteomics[3–5]. Cell-based screening approaches have the potential for discovery of cell-penetrant chemical matter that elicits a desired cellular response, and they have been instrumental in hit discovery for 37% of the first-in-class drugs approved by the US Food and Drug Administration between 1999 and 2008 (ref. 6). Recent notable successes include the tankyrase inhibitor XAV939 (ref. 7) and the porcupine inhibitor LGK974 (ref. 8), which have rekindled cell biology and drug discovery interest in WNT signaling[9].

We previously reported a series of 3,4,5-trisubstituted pyridines identified from a high-throughput cell-based reporter assay of WNT signaling; optimization to CCT251545 (**1**) (**Fig. 1a**) provided preliminary evidence for *in vivo* activity[10]. However, we recognized that identification of the molecular target(s) would accelerate further progress: for example, by enabling the discovery of proximal pharmacodynamic biomarkers with which to establish direct target engagement *in vivo*. Using a cell-based assay cascade in which WNT signaling is activated at distinct loci, we had previously established that **1** acts at or below T cell factor (TCF) in the cascade[10]. Regulation of β-catenin–TCF transcription involves recruitment or loss of DNA-binding proteins, histone modification and interaction with additional protein networks such as the Mediator complex that provide the link between gene-specific regulators and basal transcriptional machinery[11–14]. Given the complexity of these multiple networked interactions in the β-catenin–TCF locale, a candidate-based investigation to identify the molecular targets of **1** was impractical, and we therefore adopted an unbiased chemical proteomics approach.

Herein we report the molecular targets of the 3,4,5-trisubstituted pyridine series—namely the Mediator complex–associated, cyclin-dependent kinases CDK8 and CDK19—and the characterization of CCT251545 as a potent and selective chemical probe suitable for cell-based and *in vivo* exploration of the reported context-dependent roles of CDK8 and CDK19 and associated kinase module subunits in human disease and other biological settings[15–17].

RESULTS

Target identification

To identify the molecular target(s) of the 3,4,5-trisubstituted pyridine series, we prepared a set of derivatives to enable Cellular Target Profiling (evotec, https://www.evotec.com/) from cell lysates of LS174T human colon carcinoma cells that harbor an activating β-catenin mutation. Taking cognizance of the potency and structure-activity relationships of **1**, the morpholine analog **2** and the *N*-methylpiperazine analog (**3**) in a cell-based reporter assay of WNT signaling[10], we hypothesized that substitution from the terminal piperazine nitrogen of **3** would maintain activity. The *N*-propylpiperazine (**4**) demonstrated toleration of a linker along this vector, and the extended derivative **5** retained cellular potency and enabled coupling to Sepharose beads to generate an affinity matrix. LS174T cells were grown in media with different isotopically labeled amino acids; target proteins were then captured from lysates by the
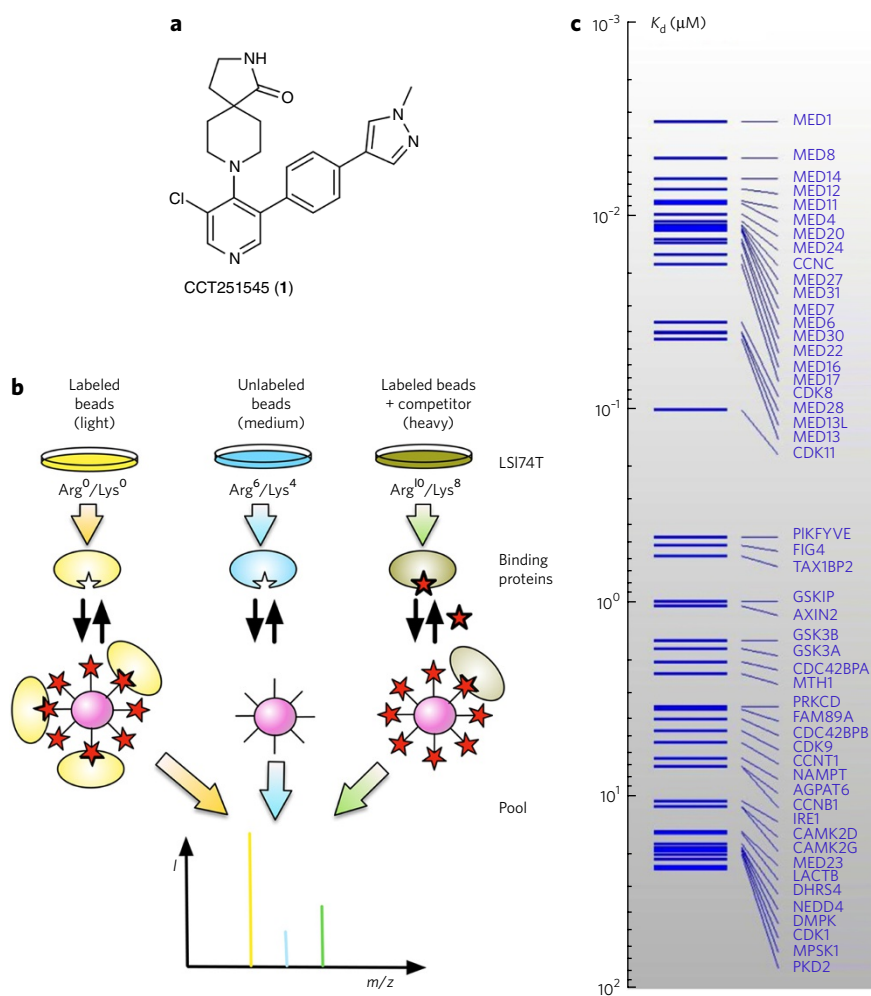
Figure 1 | Identification of the molecular targets of CCT251545. (**a**) Chemical structure of compound **1**. (**b**) LS174T cells were SILAC-encoded with normal or stable isotope–labeled arginine and lysine (Arg⁶, arginine with 6 ¹³C atoms replacing the normal ¹²C; Arg¹⁰, lysine with 6 ¹³C and 4 ¹⁵N atoms replacing the normal ¹²C and ¹⁴N; Lys⁴, lysine with 4 ²H atoms replacing the normal ¹H; Lys⁸, lysine with 6 ¹³C and 2 ¹⁵N atoms replacing the normal ¹²C and ¹⁴N; Arg⁰ and Lys⁰ denote the naturally occurring amino acids containing ¹²C, ¹⁴N and ¹H). Cell lysates (LS174T) were incubated with control beads or beads coupled to **5** in the presence of 3 nM to 30 µM of **4**, **6** or inactive control **7** (competitors). After washing, proteins that remained bound were eluted, separated by SDS-PAGE, trypsinized and analyzed by LC-MS/MS (schematic plot shows intensity, *I*, versus mass-to-charge ratio, *m/z*). (**c**) Ranked plot of proteins that selectively bound to compound **5**–conjugated beads and were displaced by compound **4**; proteins are ranked from top to bottom according to their affinities (*K*d values in µM). CDK19 is annotated as CDK11 in this figure.

compound **5** affinity matrix before displacement by unconjugated **4**, the active nonbasic indazole **6** or, as a nondisplacing control, the inactive *N*-propylpiperazine (**7**), which has a chemical structure and physicochemical properties similar to those of **4** (**Supplementary Results**, **Supplementary Table 1**). SILAC-based quantitative mass spectrometry facilitated the identification of proteins that specifically interact with immobilized compound **5** and determination of their affinities as previously described (**Fig. 1b**)[18]. In competition experiments, unconjugated analogs **4** and **6** were used at a range of concentrations (3 nM to 30 µM). Target profiling in competition with **4** revealed 53 potential target proteins, all of which showed concentration-dependent binding to the affinity matrix as well as concentration-dependent displacement by **4** with apparent *K*d values between 3 nM and 23.9 µM (**Fig. 1c** and **Supplementary Table 2**). Of these, 18 were protein kinases, suggesting a binding preference for this protein family. We also identified proteins that have been

strongly linked to WNT signaling, including AXIN2 and GSK3β; however, their affinities (*K*d ~ 1 µM, **Supplementary Table 2**) were two orders of magnitude weaker than *in vitro* cell-based reporter activities in both 7dF3 (ref. 10) and LS174T cells (**Supplementary Table 1**), suggesting that they are unlikely to mediate the observed cell-based activities. By contrast, CDK8 and CDK19 exhibited the highest affinities for compound **4** of the kinases identified in the displacement assay (*K*d = 36 and 102 nM, respectively).

CDK8, and its paralog CDK19, are transcription-regulating cyclin C–dependent kinases. CDK8 and CDK19 are components of the Mediator complex, which provides a link between transcriptional regulators, the RNA polymerase II (Pol II) transcription machinery and gene-specific transcription; CDK8 or CDK19 form a four-subunit subcomplex with cyclin C, MED12 and MED13 (commonly referred to as the kinase-module) that associates in a dynamic fashion with the rest of the Mediator complex[13,19,20]. Consistent with these observations, we identified 20 additional Mediator complex components as proteins specifically isolated with immobilized compound **5** that were competed off by compound **4** with apparent *K*d values of <100 nM (**Fig. 1c** and **Supplementary Table 2**). Competition with **6** also identified CDK8 and CD19 as high-affinity specific binding proteins in the displacement assay (*K*d = 49 and 14 nM, respectively), together with eight additional Mediator complex components (**Supplementary Fig. 1** and **Supplementary Table 3**). By contrast, the structurally similar but inactive analog **7** failed to compete with any components of the Mediator complex, including CDK8 and CDK19 (**Supplementary Table 4**).

Interestingly, both **4** and **6** interacted weakly (*K*d = 0.407–0.578 µM) with three components of the PI(3,5)P₂, regulatory complex: 1-phosphatidylinositol 3-phosphate 5-kinase (PIKFYVE), phosphatidylinositol 3,5-bisphosphate 5-phosphatase (FIG4), and tax1-binding protein 2 (TAX1BP2). However, as inactive analog **7** also interacted with the same three components (*K*d = 0.012–0.018 µM), we deduced that binding to these proteins is unlikely to contribute to cellular activity (**Fig. 1c**, **Supplementary Fig. 1** and **Supplementary Tables 2–4**).

We concluded from these results that an affinity matrix comprising immobilized compound **5** selectively binds kinases CDK8 and CDK19. Interestingly, many components of the Mediator complex remained intact during the capture protocol, although we did not observe co-purification of any transcription factors such as β-catenin–TCF or components of the core RNA Pol II machinery that have been shown to interact with the Mediator subunits[13]. Consistent with these observations, competitor compounds **4** and **6**, but not inactive control **7**, competitively displaced CDK8 or CDK19, other kinase module components, and additional Mediator complex partners from the affinity matrix (**Fig. 1c**, **Supplementary Fig. 1** and **Supplementary Tables 2–4**).

To examine the extent to which CDK8 and CDK19 binding explained the cell-based activity of the 3,4,5-trisubstituted pyridine
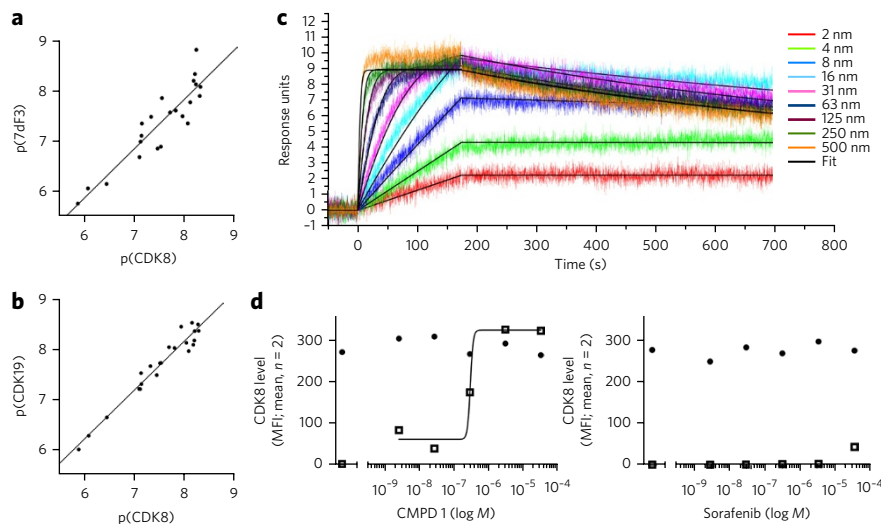
Figure 2 | Characterization of the interaction between CDK8 and CDK19 and the 3,4,5-trisubstituted pyridine series. (**a**) CDK8 binding affinity versus 7dF3 cell–based reporter potency for 22 compounds in the 3,4,5-trisubstituted pyridine series (all data shown as pIC_{50}, $R^2 = 0.83$). (**b**) CDK8 versus CDK19 binding affinity for 22 compounds in the 3,4,5-trisubstituted pyridine series (all data shown as pIC_{50}, $R^2 = 0.95$). (**c**) Direct binding of **1** to CDK8–cyclin C measured by surface plasmon resonance spectroscopy; $K_d = 2$ nM; stoichiometry = 1:1; residence time = 11 min. (**d**) CETSA analysis confirming target engagement of **1** (left), but absence of sorafenib binding (right), with CDK8 in SW620 cells. Cells were treated with **1** or sorafenib, and cell lysates were prepared for analysis after 2 h of treatment. CDK8 levels were determined using a bead-based ELISA: circles, non-heated sample; squares, sample heated at 50 °C ($n = 2$, repeat experiments; MFI, mean fluorescence intensity).

series, we compared CDK8 kinase binding affinity with our previously reported 7dF3 and LS174T cell–based TCF/LEF WNT-reporter potencies for a series of compounds of varying activity (**Fig. 2a** and **Supplementary Fig. 2**) (ref. 10). The observed correlations ($R^2 = 0.83$ and 0.85, respectively), coupled with a strong correlation between CDK8 and CDK19 binding affinity across 3,4,5-trisubstituted pyridines ($R^2 = 0.95$, **Fig. 2b**), indicated that CDK8 and/or CDK19 are major contributors to the cell-based activity in both LS174T and 7dF3 cells. Similar binding affinity for both kinases is consistent with the high sequence similarity between the CDK8 and CDK19 kinase domains; the closest nonconserved amino acid residues to the ATP binding site (Asp48, Ser80, Thr360 in CDK8; glutamic acid, alanine and asparagine, respectively, in CDK19) are remote (8–13 Å) and unlikely to directly influence ligand binding.

Confirmation of binding to CDK8 and CDK19
We used surface plasmon resonance (SPR) studies with the full-length CDK8–cyclin C complex to confirm direct target binding for **1** (**Fig. 2c**). Reporter displacement assays against full-length CDK8–cyclin C and CDK19–cyclin C complexes were also used to determine compound K_d and binding kinetics (**Supplementary Tables 5** and **6**). Cellular thermal shift analysis (CETSA)[21] confirmed high-affinity target engagement for **1** with both CDK8 and CDK19 in SW620 human colorectal cancer cells exhibiting constitutively active WNT signaling due to an inactivating *APC* mutation (**Fig. 2d** and **Supplementary Fig. 3**).

Selective pulldown of CDK8 and CDK19 from LS174T cell lysates by immobilized compound **5** is consistent with the selectivity profile of **1** when tested at 1 µM against an additional panel of 291 kinases and 55 receptors, ion channels and enzymes[10]. GSK3α and GSK3β were the only hits ($IC_{50} = 0.462$ and 0.690 µM, respectively), an observation consistent with the identification of these two kinases as weak interactors by SILAC ($K_d = 1.75$ and 1.59 µM, respectively; **Fig. 1c** and **Supplementary Table 2**). Importantly,

there was no evidence for inhibition of CDK1 through CDK7 or CDK9 in the presence of their respective cyclin partners. Taken together, SILAC-mediated target identification, kinase selectivity data, biophysical methods (both *in vitro* and in cells) and the close correlation between kinase binding affinity and cellular activity suggest that CDK8 and CDK19, likely as part of a Mediator complex, are the molecular targets of the 3,4,5-trisubstituted pyridine series.

### Type II inhibitors of CDK8 and CDK19
Interestingly, we observed that sorafenib—a reported inhibitor of CDK8 and CDK19 that was confirmed in our hands ($IC_{50} = 0.199$ and 0.206 µM, respectively) and for which X-ray crystallographic studies reveal a type II binding mode (PDB code 3RGF)[22]—did not exhibit potent cell-based activity in 7dF3 or LS174T reporter assays (**Supplementary Table 7**) and also did not demonstrate binding and stabilization of CDK8 nor CDK19 in SW620 cells by CETSA (**Fig. 2d** and **Supplementary Fig. 3**). We therefore investigated whether other type II inhibitors of CDK8 and CDK19 could be translated to cell-based assays of WNT signaling. Biochemical screening of available clinical and preclinical kinase inhibitors with chemical structures consistent with a type II binding mode revealed potent binding activity for ponatinib (Iclusig), a BCR-ABL inhibitor marketed for relevant leukemias[23], and linifanib, a potent inhibitor of receptor tyrosine kinases in clinical studies[24]. Similar to what was seen with sorafenib, we noted that the *in vitro* potency of linifanib versus CDK8–cyclin C and CDK19–cyclin C ($IC_{50} = 0.014$ and 0.024 µM, respectively) did not translate either to potent inhibition of TCF reporter activity in 7dF3 or LS174T cells ($IC_{50} = 1.29$ and 5.170 µM, respectively) or to CDK8 and CDK19 binding in SW620 cells (CETSA), despite reports in the literature of its potent cell-based activity against other kinase targets[25,26]. For ponatinib, we observed improved translation to cell-based TCF/LEF reporter activity; however, CETSA analysis in SW620 cells revealed minimal stabilization of CDK8 or CDK19 at 0.30 µM—a 21-fold and 13-fold drop-off compared to *in vitro* potency—whereas compound **1** showed >50% stabilization at 0.30 µM (**Supplementary Table 7** and **Supplementary Fig. 3**). Notably, linifanib and ponatinib exhibited longer residence times than sorafenib and **1** versus CDK8 (295, 512, 52 and 43 min, respectively; **Supplementary Table 5**) and versus CDK19 (166, 413, 106 and 86 min, respectively; **Supplementary Table 6**). Thus the better translation to cell-based potency observed for **1** cannot be attributed to longer target residence time. Cell-penetrant type II kinase inhibitors do not compete with ATP[27] and are therefore less prone to reduced potency in cell-based assays; we were therefore interested in exploring differences in CDK8-binding mode between **1** and sorafenib.

Structure of CDK8–cyclin C in complex with CCT251545
To investigate the mode of binding of 3,4,5-trisubstituted pyridines to CDK8, and its potential differences from the reported sorafenib type II binding mode, we obtained the crystal structure of **1** in complex with the kinase domain of CDK8 and cyclin C at 2.6-Å resolution (PDB code 5BNJ; **Fig. 3a** and **Supplementary Table 8**). In this structure, CDK8 is observed in complex with cyclin C, with the ligand occupying the ATP-binding site. Binding of **1** to the kinase
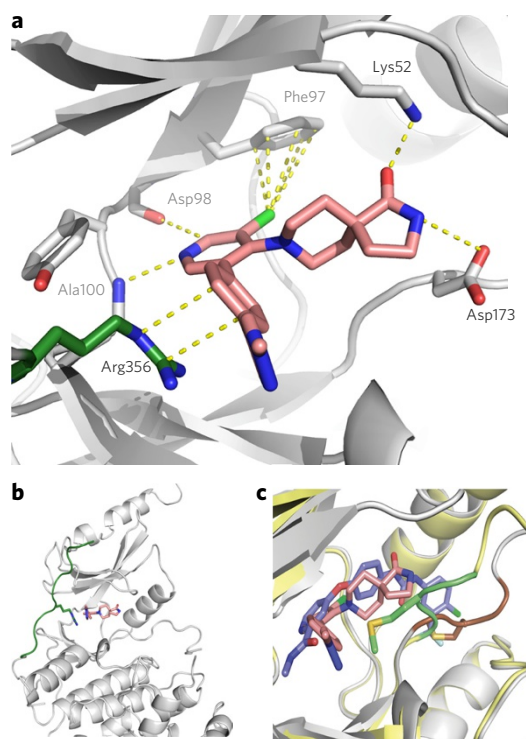
Figure 3 | X-ray crystal structural analysis of compound 1 bound to CDK8–cyclin C. (**a**) Protein crystal structure of CDK8–cyclin C bound to **1** (PDB code 5BNJ); compound **1** is shown in pink and CDK8 protein in gray, with Arg356 highlighted in green; key interactions are depicted by yellow dashed lines and key residues annotated. Residues Lys26, Val27, Gly28, Arg29 and Gly30 have been cropped for clarity. (**b**) Protein crystal structure of CDK8–cyclin C bound to **1**, showing insertion of C-terminal chain (green) into the hinge region of CDK8. (**c**) Protein crystal structure of CDK8 bound to sorafenib (PDB code 3RGF; ref. 22; ligand is in violet, protein backbone in light yellow and DMG motif in light green) overlaid with compound **1** bound to CDK8 (ligand in pink, protein backbone in gray and DMG motif in light brown) showing a DMG-out orientation of the activation loop in the sorafenib-bound structure that is consistent with a type II binding mode.

hinge region involves a hydrogen bond acceptor interaction of the pyridine nitrogen with the NH of Ala100; the observed electron density also supports an interaction between C2-H of the pyridine ring and the carbonyl of Asp98. The 3-chloro substituent of the pyridine ring stacks against gatekeeper residue Phe97, and the amide of the spirolactam moiety bridges between the catalytic Lys52 and residue Asp173 of the DMG motif located at the N terminus of the activation loop. Of particular note, we observe a torsion between the plane of the piperidine and pyridine rings, which is consistent with our observation that such a conformation is important for activity of the 3,4,5-trisubstituted pyridine series in cell-based reporter assays[10]. The C5-phenylpyrazole substituent occupies the solvent channel, consistent with the maintained potency of **5**, which bears an extended linker along this vector. Interestingly, the extended C-terminal chain of CDK8 is observed to reinsert adjacent to the hinge region in the presence of **1**, with the guanidine side chain of Arg356 forming a cation-*pi* interaction with phenyl ring of the ligand (**Fig. 3a,b**). This interaction is consistent with previously reported structure-activity relationships whereby strongly electron-withdrawing substituents on the phenyl ring abrogate activity[10]. We postulate that this unusual C-terminal Arg356 insertion into the hinge region may contribute to the exquisite kinase selectivity of **1**. Notably, the binding mode of **1** is significantly different from that in the published structure of sorafenib with CDK8 (PDB code 3RGF)[22], where a DMG-out orientation of

the activation loop is observed, consistent with a type II binding mode, and where the extended C-terminal tail, including Arg356, is present in the crystallography construct but is not resolved (**Fig. 3c**). We hypothesize that the relatively poor translation into 7dF3 and LS174T cell–based reporter activity observed for sorafenib and other type II CDK8 inhibitors may be a consequence of their type II binding mode, suggesting that intracellular CDK8 is trapped in a tightly bound active conformation either in a Mediator complex or in a free four-subunit kinase module, with slow equilibration to inactive kinase conformations. This notion is consistent with our observation that MED12, MED13 and an intact Mediator complex were captured by the affinity matrix containing compound **5**.

Compound-induced gene expression changes

We next explored how gene expression changes induced by **1** correlated with those caused by silencing of *CDK8* and/or *CDK19*. Colo205 human colorectal cancer cells harboring *CDK8* amplification[28] were stably transduced with a doxycycline (dox)-inducible shRNA-expressing plasmid targeting *CDK8* or a stable shRNA targeting *CDK19*. Following expression of the shRNAs, we observed a reduction in TCF-dependent reporter transcription, consistent with the observed effect of **1** on this cell line (**Fig. 4a** and **Supplementary Fig. 4**). A similar reduction in TCF-dependent transcription also occurred in 7dF3 cells following treatment with enzymatically synthesized siRNA (esiRNA) for *CDK8* or *CDK19* (**Supplementary Fig. 5**). CDK8 protein was expressed from a dox-inducible promoter in a HEK293 cell line with low basal levels of TCF-dependent transcription. Wild-type, but not kinase-dead, CDK8 increased basal levels of TCF-reporter expression by two-fold (**Fig. 4b**). Taken together, these data indicate that expression of an enzymatically active CDK8 is necessary and sufficient for activating a fraction of total β-catenin–TCF-dependent transcription.

We next examined a 3D culture model of mouse intestinal-derived organoids expressing a transgenic dox-inducible mutant β-catenin[29]. In this model, loss of activated β-catenin expression following removal of dox results in reduced WNT signaling with characteristic decreased expression of *Axin2*, *Ascl2*, *Myc* and *Tiam1* and increased expression of the enterocyte differentiation marker *Car4*, as determined by qRT-PCR (**Fig. 5a**). Treatment with **2**, a close analog of **1** with an equivalent pharmacological and kinase selectivity profile (**Supplementary Tables 1, 9** and **10**), produced a gene expression signature consistent with WNT signaling inhibition following loss of mutant β-catenin expression (**Fig. 5a**).

To identify broader patterns in transcriptional responses to our CDK8 and CDK19 inhibitors, gene expression microarray studies were performed using mRNA prepared from the same mouse cell organoids expressing mutant β-catenin. The organoids were treated with **2**, analog **6** (with an equivalent pharmacological and kinase selectivity profile to **2**) or inactive analog **8** (**Supplementary Tables 9** and **11**). Loss of activated β-catenin resulted in significantly ($P < 0.001$) altered expression of 78 genes (**Supplementary Figs. 6–8**). Consistent with inhibition of WNT signaling, 31 of the 78 genes, including *Axin2*, *Ascl2* and *Myc*, are known targets of WNT signaling. In agreement with the notion that our optimized 3,4,5-trisubstituted pyridines would not be general inhibitors of transcription, treatment with compound **2** or **6** resulted in significantly ($P < 0.001$) altered expression of only 34 or 219, genes, respectively (**Supplementary Figs. 6** and **7**). Importantly, inactive control **8** did not elicit any of the significant gene expression changes observed with **2** or **6**. Comparison of these data with the expression profile resulting from loss of activated β-catenin confirmed that compounds **2** and **6** each inhibit WNT signaling (**Fig. 5a** and **Supplementary Fig. 7a**). Treatment with either active compound, but not inactive analog **8**, also induced an additional set of transcriptional changes not shared by β-catenin removal. This included a 'stress response' gene expression signature that has been linked to
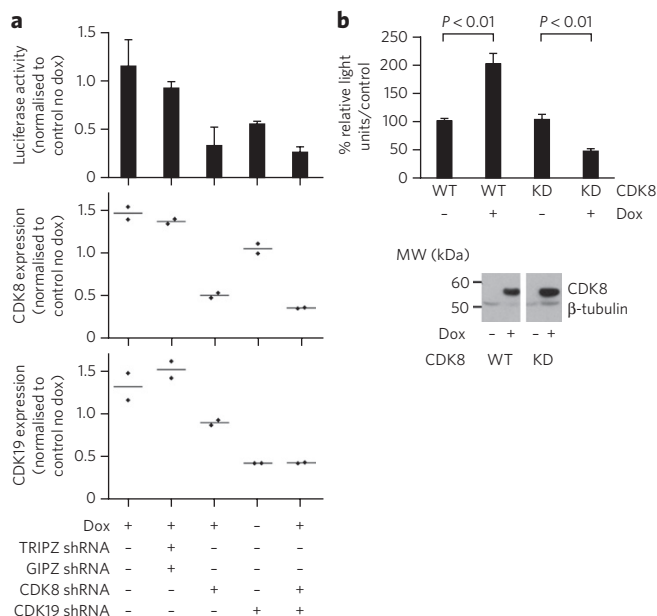
Figure 4 | Altered CDK8 and/or CDK19 expression affects WNT-regulated transcription. (**a**) Reduced expression of CDK8, CDK19 or both CDK8 and CDK19 resulting from shRNA expression inhibits TCF/LEF reporter gene transcription in Colo205 cells (top graph; data represent mean values ± s.e.m., n = 3 independent repeat experiments). Reduced CDK8 and CDK19 expression (middle and bottom graph, respectively) were confirmed by quantitative RT-PCR. Data are plotted relative to those for parent cells cultured in the absence of doxycycline (dox; n = 2 independent repeat experiments). Cells were treated for 10 d with 5 µg/ml dox before reporter or mRNA levels were measured (control dox, parent Colo205 cells; TRIPZ-GIPZ, cells expressing both a TRIPZ dox-inducible non-targeting shRNA and a GIPZ constitutively expressed non-targeting shRNA; CDK8, cells expressing a dox-inducible CDK8 shRNA; CDK19, cells expressing a constitutive CDK19 shRNA). (**b**) Dox-inducible expression of a wild-type (WT) or a kinase-dead (D173A; KD) CDK8 variant (immunoblot, below β-tubulin loading control; **Supplementary Fig. 16**) induces TCF-dependent reporter transcription in HEK293 cells (plot, above; n = 4 per group; t-test ± s.e.m. shown).

NRF2 signaling and is consistent with literature reports that CDK8 and CDK19 may be involved in regulating stress response pathways (**Supplementary Figs. 7** and **8**) (ref. 30).

A further analysis of changes in mRNA abundance was also carried out in LS174T and Colo205 human colorectal cancer cells treated with **1** or **6** (**Supplementary Fig. 9**). Comparing the mRNAs that are differentially expressed following compound treatment to those modulated by overexpression of dominant-negative TCF4 or after depletion of β-catenin by shRNA in LS174T cells[31] again identified a significant overlap (**Fig. 5b**). As in the organoids, not all of the changes in mRNA abundance resulting from compound treatment could be accounted for by modulation of WNT signaling. The overlap between the transcripts affected in different cell lines and those modulated in response to our compounds was also incomplete, which is unsurprising given the potentially pleiotropic effects of CDK8 and CDK19 modulation and the different genetic backgrounds of the cell lines selected for analysis. However, when we compared enrichment of transcription factor–binding sites in genes encoding transcripts significantly altered in abundance, we found more similarity between the effects of compound treatment between LS174T and Colo205 cells (**Fig. 5b** and **Supplementary Data Set 1**). Of note, we identified enrichment of genes regulated by TCF4, LEF1 and additional transcription factors reliant on the Mediator complex and CDK8 or CDK19 (**Supplementary Data Set 1**).
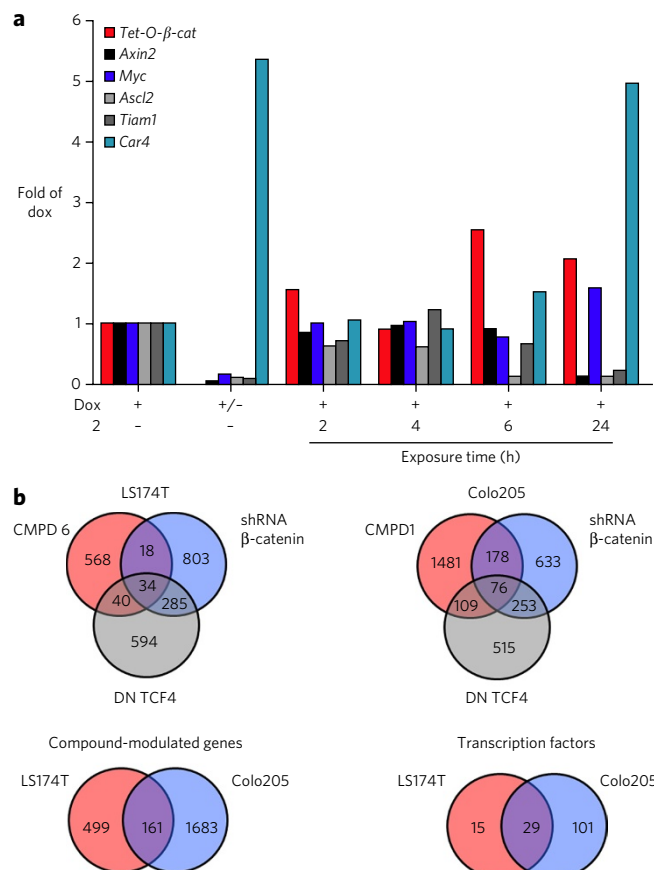
Figure 5 | Gene transcript profiling following inhibition of WNT signaling resulting from loss of β-catenin or following treatment with 3,4,5-trisubstituted pyridines. (**a**) Gene expression in cultured intestinal organoids established from mice expressing a doxycycline (dox)-inducible mutant β-catenin (Tet-O-Δ1–89–β-catenin). Organoids induced with 2 mg/ml dox were treated with **2** (2 µM), and transcript levels for WNT target genes (*Myc*, *Ascl2*, *Tiam1* or *Axin2*), the dox-inducible transgene (*Tet-O–β-Catenin* (*Tet-O–β-Cat*)) or the enterocyte differentiation marker *Car4* were then quantified (plot shows a representative experiment; n = 1). (**b**) Changes in transcript abundance were profiled in LS174T cells in response to a 4- or 24-h treatment with compound **6** (715 nM: IC90 for inhibition of the luciferase reporter) and in, Colo205 cells in response to a 2 or 6 h treatment with compound **1** (350 nM). The abundance of 660 and 1,844 transcripts were significantly altered in response to treatment of LS174T or Colo205 cells, respectively. The upper Venn diagrams show the significant overlap between those transcripts whose expression was altered as a result of compound treatment and those affected by modulation of key WNT regulators, β-catenin or TCF4 (published data[31]; DN TCF4, dominant-negative TCF4). The lower Venn diagrams show the overlap between transcripts modulated as a result of treatment of cells with compounds **1** or **6** (left) and between transcription factors that bind modulated genes in LS174T and Colo205 cells (right).

These included the STAT family of transcription factors[32], HIF1a[33], serum response factor (SRF) and SRF-dependent transcription factors such as JUN[34], and also NRF2, which was detected in the organoid expression profiling experiments (**Supplementary Figs. 7** and **8**). Pathway analysis (**Supplementary Data Set 2**) also revealed enrichment of transcripts from genes that encode proteins involved in pathways or processes regulated or influenced by CDK8 or CDK19 and the Mediator complex—such as WNT, TGFβ, the inflammation and immune response, cell adhesion, the epithelial-to-mesenchymal transition and development.
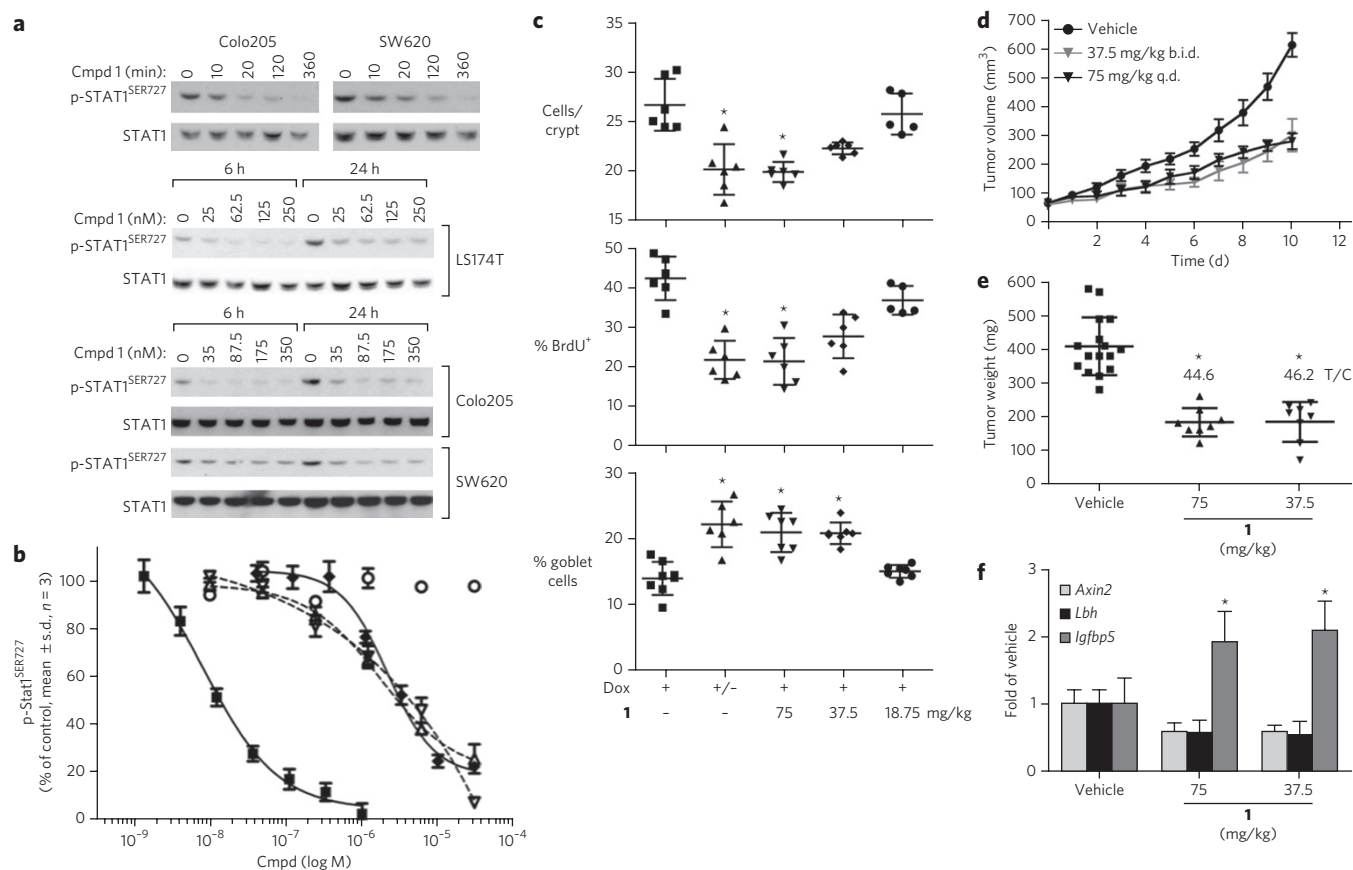
Figure 6 | Biomarker modulation and therapeutic effects of compound 1 in human cancer cell lines and *in vivo* animal models. (a) Above, Colo205 and SW620 cells were treated for 10–360 min with compound **1** (350 nM: 10× reporter IC_{50}). Below, LS174T, Colo205 and SW620 cells were treated for 6 and 24 h with 1–10× their reporter IC_{50} values. Proteins were measured by immunoblotting (**Supplementary Fig. 16**). **(b)** p-STAT1^{SER727} levels were determined following treatment of SW620 cells with **1** (squares; IC_{50} = 9 nM), sorafenib (open circles; IC_{50} = not determined), ponatinib (upright triangles; IC_{50} = 2,800 nM), linifanib (inverted triangles; IC_{50} = 1,800 nM) and less active control **9** (diamonds; IC_{50} = 2,200 nM, **Supplementary Table 9**; mean ± s.d.; n = 3 independent repeat experiments). **(c)** Tet-O–β-catenin mice with hyperplastic intestinal epithelium following 6 d of doxycycline (dox) treatment were administered **1** twice a day for 2 d. Dox withdrawal was a positive control for loss of WNT signaling. Changes in crypt length, cell proliferation and differentiation (mean ± s.d.; n = 8 per group) were quantified; * indicates $P < 0.0003$ by Kruskal-Wallis test and $P < 0.01$ after with Dunn's *post-hoc* test. **(d)** CD1(nu/nu) mice bearing MMTV-WNT-1 tumors were treated with compound **1** for 10 d, and tumor volume was estimated from measured dimensions (mean ± s.d.; n = 8; paired controls were set up for each treatment condition). b.i.d., twice a day; q.d., once a day. **(e,f)** MMTV-WNT-1 tumors were harvested from CD1(nu/nu) mice (mean ± s.d.; n = 8 per group; *$P < 0.01$ by Kruskal-Wallis and $P < 0.05$ after Dunn's *post hoc* test:) after 10 d of treatment and then either they were weighed **(e)** or their mRNA was extracted and the expression of WNT target genes or *Igfbp5* (involution marker[40]) determined by qRT-PCR (mean ± s.d.; n = 8 per group) **(f)**.

Overall, the gene expression changes we observed are consistent with our previous report identifying the 3,4,5-trisubstituted pyridine series as inhibitors of WNT signaling in the TCF locale[10]. Furthermore, the altered levels of transcripts from genes influenced by transcription factors known to be regulated by the Mediator complex and CDK8 or CDK19 are consistent with our compounds affecting CDK8- and CDK19-regulated gene transcription beyond WNT signaling (**Supplementary Data Sets 1** and **3**)[35,36].

Confirmation of cell-based target engagement by CCT251545

In our microarray profiling experiments, we detected changes in transcript levels that are likely to result from alterations to STAT-regulated signaling (**Supplementary Data Set 1**), consistent with a recent report[32] of CDK8-mediated phosphorylation of STAT1 (signal transducer and activator of transcription 1) at STAT1^{SER727}. Given these observations, we explored the effect of **1** on STAT1^{SER727} phosphorylation in cells. Pleasingly, we demonstrated potent time- and concentration-dependent reduction of phospho-STAT1^{SER727} levels in the three human colorectal cancer cell lines used earlier (Colo205, LS174T and SW620). When tested at a concentration 10 times its IC_{50} in the respective cell-based reporter assay, **1** reduced

phosphorylation at STAT1^{SER727} within 10–20 min of treatment, with sustained inhibition at 6 and 24 h. In addition, at 6 and 24 h, **1** reduced phospho-STAT1^{SER727} levels at concentrations consistent with those that reduced WNT-reporter activity in the same cell lines (**Fig. 6a**).

CDK8 has been reported to regulate the basal transcriptional machinery through phosphorylation of the C-terminal domain (CTD) of RNA polymerase II (POLR2A^{SER2} and POLR2A^{SER5})[37] and also to phosphorylate E2F1^{SER375}, inhibiting its repressive activity toward β-catenin[38]. We did detect decreased POLR2A$^{SER2/5}$ phosphorylation following treatment of SW620 cells with **1**, although total POLR2A was also decreased to a comparable extent. In the same experiment, STAT1^{SER727} phosphorylation was potently reduced by **1** but not by the inactive analog **7**; importantly, total STAT1 levels were unaffected. We did not detect reduced E2F1^{SER375} phosphorylation following treatment of SW620 cells with a high concentration of **1** that did inhibit phospho-STAT1^{SER727} in the same samples (**Supplementary Fig. 10**). Thus, of the three reported substrates of CDK8 tested in our models, we found phosphorylation of STAT1^{SER727} to be the most robust and reliable target engagement biomarker of CDK8 inhibition by **1**.

Interestingly, we did not observe significant modulation of phospho-STAT1^{SER727} levels in SW620 cells treated with sorafenib, ponatinib or linifanib at concentrations at which treatment with **1** does lead to a significant reduction in phosphorylation, as measured both by bead-based ELISA and by immunoblotting (**Fig. 6b** and **Supplementary Fig. 11**). Indeed, ponatinib and linifanib are significantly less potent than **1** (phospho-STAT1^{SER727} IC$_{50}$ = 2,800, 1,800 and 9 nM, respectively), whereas sorafenib had a minimal effect even at the highest concentration tested (10 μM). These observations are consistent with our earlier suggestion that type II inhibitors of CDK8 and CDK19, including ponatinib, are less able to engage these kinases in the cellular context.

In vivo activity of CCT251545 in animal models

To assess the *in vivo* activity of **1**, we developed an animal model of intestinal hyperplasia dependent upon the expression of a dox-inducible mutant β-catenin transgene[29]. Oral dosing of **1** for 2 d (75, 37.5 and 18.75 mg/kg twice a day) dose-dependently reduced the length of hyperplastic crypts, with the maximum effect similar to that of the removal of dox. We observed a concomitant reduction in proliferation and increased cell differentiation in goblet cells, as quantified by BrdU and Alcian Blue staining, respectively (**Fig. 6c**). We also detected a WNT gene expression signature (**Supplementary Fig. 12**) consistent with that observed for **2** in mouse β-catenin–dependent intestinal organoids (**Fig. 5a**) and also for **2** and **6** when tested *in vivo* in the same model of intestinal hyperplasia bearing a dox-inducible mutant β-catenin transgene (**Supplementary Fig. 13 and 14**). Taken together, these data substantiate the pharmacological equivalence of compounds **1**, **2** and **6**.

The above reversal by our compounds of intestinal hyperplasia phenotypes induced by mutant β-catenin prompted us to examine the response to **1** in two different WNT-dependent tumor models. First, in MMTV-WNT-1–induced mouse breast cancer allografts transplanted into athymic mice, treatment with **1** (75 and 37.5 mg/kg once or twice a day, respectively) caused a decrease in tumor growth rate (**Fig. 6d,e**). We also detected concomitant reduction in the expression of the WNT target genes *Axin2* and *Lbh*, and induction of *Igfbp5*, a negatively regulated target of the WNT pathway whose expression is associated with tumor regression[39,40]. Altered expression of all three genes was significant by Kruskal-Wallis nonparametric ANOVA test ($P < 0.05$), although only decreased expression of *Igfbp5* retained significance ($P < 0.05$) when corrected for multiple testing using Dunn's *post hoc* test (**Fig. 6f**). In addition, compound **1** inhibited the growth of *APC*-mutant SW620 human colorectal cancer cells (GI$_{50}$ (concentration required to inhibit cell growth by 50% following continuous compound exposure for 14 d) = 140 nM; **Supplementary Fig. 15**), and treatment of athymic mice bearing established SW620 human colorectal cancer xenografts with **1** (70 mg/kg once a day for 14 d) inhibited tumor growth, with a 70% reduction in final tumor weight relative to treatment with vehicle control (**Supplementary Fig. 15**). We also observed a concomitant reduction in phospho-STAT1^{SER727} in tumor tissue (**Supplementary Fig. 15**). Plasma and tumor concentrations of **1** were measured at 2 h (2,525 ± 921 nM and 1,598 ± 324 nM, respectively) and at 6 h (188 ± 64 nM and 639 ± 115 nM, respectively) after the last dose, demonstrating exposures above the cell-based GI$_{50}$ at these time points.

DISCUSSION

CDK8 resides on a region of chromosome 13 known to undergo a gain of gene copy number in ~60% of colorectal cancers, and inducible shRNA-mediated knockdown of *CDK8* reduces the growth of HT29 and Colo205 human colorectal cancer tumor xenografts that harbor an amplified *CDK8* gene[41]. In addition, expression of wild-type CDK8 transforms NIH3T3 cells, whereas expression of a kinase-dead mutant does not, consistent with *CDK8*'s putative kinase-dependent role as an oncogene[28]. Furthermore, there are reports that CDK8

expression correlates with β-catenin activation in colon and gastric cancers and with increased mortality in colorectal, breast and ovarian cancers[42–44] and that CDK8 is overexpressed and essential for cell proliferation in melanoma[45]. These various results, incorporating data obtained through the use of RNAi and other biological perturbation, are consistent with *CDK8* acting as a kinase-dependent driver oncogene in these settings and point to the need for high-quality chemical probes[46,47] to further explore the biological roles of CDK8 and CDK19 in various biological and pathological contexts, as well as to uncover the potential utility of small-molecule inhibitors of CDK8 and CDK19 for the treatment of cancer and other human diseases.

Cortistatin A[48] was the first reported ligand for CDK8 and CDK19, and recent patent disclosures signpost an emerging interest in CDK8 inhibitors. A co-crystal structure of the type II kinase inhibitor sorafenib with CDK8–cyclin C has been reported[22], and subsequent elegant studies examined the binding kinetics of fragment-like CDK8 ligands[49].

Here we demonstrate that the 3,4,5-trisubstituted pyridine CCT251545 (**1**) has the attributes of a potent and selective chemical probe for CDK8 and CDK19. Supported by a range of other evidence provided here, the identification of CDK8 and CDK19, along with their cognate Mediator complex partners, as the only proteins from cell lysates that bind with high avidity to an affinity matrix comprising the close analog **5** provides strong evidence to reinforce the binding selectivity of this compound class in the cellular context. Protein X-ray crystallography studies of **1** in complex with CDK8–cyclin C reveal an unusual protein-binding conformation that may explain the observed kinase selectivity and enable the design of alternative CDK8- and CDK19-selective scaffolds. These studies provide a further example of potent and selective kinase inhibition via a type 1 binding mode[50].

In contrast to the type II inhibitors tested here, compound **1** displays good translation to cell-based activity, including inhibition of STAT1^{SER727} phosphorylation as a useful target engagement and pharmacodynamic biomarker of CDK8 inhibition. Furthermore, compound **1** modulates WNT-dependent gene mRNA abundance in several *in vitro* cell models and in mouse β-catenin–dependent intestinal organoids; thus it broadly phenocopies the changes seen in levels of selected transcripts following inhibition of WNT signaling by loss of activated β-catenin, consistent with our previous report that the 3,4,5-trisubstituted pyridine series acts at the TCF locale[10]. Also, while these compounds are not general transcriptional modulators, they clearly demonstrate both positive and negative effects on gene transcription that extend beyond WNT signaling and are related to additional on-target effects of modulating CDK8 and CDK19. Compound **1** inhibits the growth of MMTV-WNT-1 breast cancers transplanted from genetically engineered mice as well as *APC*-mutant SW620 human colorectal cancer xenografts, in which we also demonstrated CDK8 target engagement through concomitant reduction in levels of phospho-STAT^{SER727}, thereby establishing a link between CDK8 inhibition and WNT pathway modulation in the *in vivo* context. Although these initial data appear promising, the effects of **1** across multiple pathways regulated by CDK8 and CDK19 indicate that more extensive pharmacologic studies and safety-profile characterization will be required to substantiate whether potent and selective inhibitors of CDK8 and CDK19 inhibitors have potential as therapeutics for the treatment of cancer and other human diseases. Given the role of WNT signaling in stem cell biology, it will also be of interest to assess the impact of CDK8 and CDK19 inhibitors on the fate of cancer stem cells.

METHODS

Methods and any associated references are available in the online version of the paper.

References

1. Eggert, U.S. The why and how of phenotypic small-molecule screens. *Nat. Chem. Biol.* **9**, 206–209 (2013).
2. Blagg, J. & Workman, P. Chemical biology approaches to target validation in cancer. *Curr. Opin. Pharmacol.* **17**, 87–100 (2014).
3. Fisher, M. & Nelson, A. The chemical genetic approach: the interrogation of biological mechanisms with small molecule probes. in *New Frontiers in Chemical Biology: Enabling Drug Discovery* (ed. Bunnage, M.E.) 1–28 (Royal Society of Chemistry, 2011).
4. Bantscheff, M. & Drewes, G. Chemoproteomic approaches to drug target identification and drug profiling. *Bioorg. Med. Chem.* **20**, 1973–1978 (2012).
5. Ong, S.E. *et al.* Identifying the proteins to which small-molecule probes and drugs bind in cells. *Proc. Natl. Acad. Sci. USA* **106**, 4617–4622 (2009).
6. Swinney, D.C. & Anthony, J. How were new medicines discovered? *Nat. Rev. Drug Discov.* **10**, 507–519 (2011).
7. Huang, S.M. *et al.* Tankyrase inhibition stabilizes axin and antagonizes Wnt signalling. *Nature* **461**, 614–620 (2009).
8. Liu, J. *et al.* Targeting Wnt-driven cancer through the inhibition of Porcupine by LGK974. *Proc. Natl. Acad. Sci. USA* **110**, 20224–20229 (2013).
9. Kahn, M. Can we safely target the WNT pathway? *Nat. Rev. Drug Discov.* **13**, 513–532 (2014).
10. Mallinger, A. *et al.* Discovery of potent, orally bioavailable, small-molecule inhibitors of WNT signaling from a cell-based pathway screen. *J. Med. Chem.* **58**, 1717–1735 (2015).
11. Clevers, H. Wnt/beta-catenin signaling in development and disease. *Cell* **127**, 469–480 (2006).
12. Angers, S. & Moon, R.T. Proximal events in Wnt signal transduction. *Nat. Rev. Mol. Cell Biol.* **10**, 468–477 (2009).
13. Carlsten, J.O., Zhu, X. & Gustafsson, C.M. The multitalented Mediator complex. *Trends Biochem. Sci.* **38**, 531–537 (2013).
14. Kim, S., Xu, X., Hecht, A. & Boyer, T.G. Mediator is a transducer of Wnt/beta-catenin signaling. *J. Biol. Chem.* **281**, 14066–14075 (2006).
15. Allen, B.L. & Taatjes, D.J. The Mediator complex: a central integrator of transcription. *Nat. Rev. Mol. Cell Biol.* **16**, 155–166 (2015).
16. Schiano, C., Casamassimi, A., Vietri, M.T., Rienzo, M. & Napoli, C. The roles of mediator complex in cardiovascular diseases. *Biochim. Biophys. Acta* **1839**, 444–451 (2014).
17. Schiano, C. *et al.* Involvement of Mediator complex in malignancy. *Biochim. Biophys. Acta* **1845**, 66–83 (2014).
18. Sharma, K. *et al.* Proteomics strategy for quantitative protein interaction profiling in cell extracts. *Nat. Methods* **6**, 741–744 (2009).
19. Nemet, J., Jelicic, B., Rubelj, I. & Sopta, M. The two faces of Cdk8, a positive/negative regulator of transcription. *Biochimie* **97**, 22–27 (2014).
20. Conaway, R.C. & Conaway, J.W. Function and regulation of the Mediator complex. *Curr. Opin. Genet. Dev.* **21**, 225–230 (2011).
21. Martinez Molina, D. *et al.* Monitoring drug target engagement in cells and tissues using the cellular thermal shift assay. *Science* **341**, 84–87 (2013).
22. Schneider, E.V. *et al.* The structure of CDK8/CycC implicates specificity in the CDK/cyclin family and reveals interaction with a deep pocket binder. *J. Mol. Biol.* **412**, 251–266 (2011).
23. Lipton, J.H. *et al.* Comparative efficacy of tyrosine kinase inhibitor treatments in the third-line setting, for chronic-phase chronic myelogenous leukemia after failure of second-generation tyrosine kinase inhibitors. *Leuk. Res.* **39**, 58–64 (2015).
24. Cainap, C. *et al.* Linifanib versus sorafenib in patients with advanced hepatocellular carcinoma: results of a randomized phase III trial. *J. Clin. Oncol.* **33**, 172–179 (2015).
25. Gozgit, J.M. *et al.* Ponatinib (AP24534), a multitargeted pan-FGFR inhibitor with activity in multiple FGFR-amplified or mutated cancer models. *Mol. Cancer Ther.* **11**, 690–699 (2012).
26. Shankar, D.B. *et al.* ABT-869, a multitargeted receptor tyrosine kinase inhibitor: inhibition of FLT3 phosphorylation and signaling in acute myeloid leukemia. *Blood* **109**, 3400–3408 (2007).
27. Garuti, L., Roberti, M. & Bottegoni, G. Non-ATP competitive protein kinase inhibitors. *Curr. Med. Chem.* **17**, 2804–2821 (2010).
28. Firestein, R. *et al.* CDK8 is a colorectal cancer oncogene that regulates beta-catenin activity. *Nature* **455**, 547–551 (2008).
29. Jardé, T. *et al.* In vivo and in vitro models for the therapeutic targeting of Wnt signaling using a Tet-OΔN89beta-catenin system. *Oncogene* **32**, 883–893 (2013).
30. Krasley, E., Cooper, K.F., Mallory, M.J., Dunbrack, R. & Strich, R. Regulation of the oxidative stress response through Slt2p-dependent destruction of cyclin C in *Saccharomyces cerevisiae*. *Genetics* **172**, 1477–1486 (2006).
31. Mokry, M. *et al.* Integrated genome-wide analysis of transcription factor occupancy, RNA polymerase II binding and steady-state RNA levels identify differentially regulated functional gene classes. *Nucleic Acids Res.* **40**, 148–158 (2012).
32. Bancerek, J. *et al.* CDK8 kinase phosphorylates transcription factor STAT1 to selectively regulate the interferon response. *Immunity* **38**, 250–262 (2013).
33. Galbraith, M.D. *et al.* HIF1A employs CDK8-mediator to stimulate RNAPII elongation in response to hypoxia. *Cell* **153**, 1327–1339 (2013).
34. Donner, A.J., Ebmeier, C.C., Taatjes, D.J. & Espinosa, J.M. CDK8 is a positive regulator of transcriptional elongation within the serum response network. *Nat. Struct. Mol. Biol.* **17**, 194–201 (2010).
35. Galbraith, M.D., Donner, A.J. & Espinosa, J.M. CDK8: a positive regulator of transcription. *Transcription* **1**, 4–12 (2010).
36. Alarcón, C. *et al.* Nuclear CDKs drive Smad transcriptional activation and turnover in BMP and TGF-beta pathways. *Cell* **139**, 757–769 (2009).
37. Rickert, P., Seghezzi, W., Shanahan, F., Cho, H. & Lees, E. Cyclin C/CDK8 is a novel CTD kinase associated with RNA polymerase II. *Oncogene* **12**, 2631–2640 (1996).
38. Morris, E.J. *et al.* E2F1 represses beta-catenin transcription and is antagonized by both pRB and CDK8. *Nature* **455**, 552–556 (2008).
39. Rieger, M.E., Sims, A.H., Coats, E.R., Clarke, R.B. & Briegel, K.J. The embryonic transcription cofactor LBH is a direct target of the Wnt signaling pathway in epithelial development and in aggressive basal subtype breast cancers. *Mol. Cell. Biol.* **30**, 4267–4279 (2010).
40. Liu, B.Y. *et al.* Mammary tumor regression elicited by Wnt signaling inhibitor requires IGFBP5. *Cancer Res.* **72**, 1568–1578 (2012).
41. Adler, A.S. *et al.* CDK8 maintains tumor dedifferentiation and embryonic stem cell pluripotency. *Cancer Res.* **72**, 2129–2139 (2012).
42. Firestein, R. *et al.* CDK8 expression in 470 colorectal cancers in relation to beta-catenin activation, other molecular alterations and patient survival. *Int. J. Cancer* **126**, 2863–2873 (2010).
43. Kim, M.Y., Han, S.I. & Lim, S.C. Roles of cyclin-dependent kinase 8 and beta-catenin in the oncogenesis and progression of gastric adenocarcinoma. *Int. J. Oncol.* **38**, 1375–1383 (2011).
44. Porter, D.C. *et al.* Cyclin-dependent kinase 8 mediates chemotherapy-induced tumor-promoting paracrine activities. *Proc. Natl. Acad. Sci. USA* **109**, 13799–13804 (2012).
45. Kapoor, A. *et al.* The histone variant macroH2A suppresses melanoma progression through regulation of CDK8. *Nature* **468**, 1105–1109 (2010).
46. Frye, S.V. The art of the chemical probe. *Nat. Chem. Biol.* **6**, 159–161 (2010).
47. Workman, P. & Collins, I. Probing the probes: fitness factors for small molecule tools. *Chem. Biol.* **17**, 561–577 (2010).
48. Cee, V.J., Chen, D.Y., Lee, M.R. & Nicolaou, K.C. Cortistatin A is a high-affinity ligand of protein kinases ROCK, CDK8, and CDK11. *Angew. Chem. Int. Ed. Engl.* **48**, 8952–8957 (2009).
49. Schneider, E.V., Bottcher, J., Huber, R., Maskos, K. & Neumann, L. Structure-kinetic relationship study of CDK8/CycC specific compounds. *Proc. Natl. Acad. Sci. USA* **110**, 8081–8086 (2013).
50. Huang, D., Zhou, T., Lafleur, K., Nevado, C. & Caflisch, A. Kinase selectivity potential for inhibitors targeting the ATP binding site: a network analysis. *Bioinformatics* **26**, 198–204 (2010).

Author contributions

J.B., A.M., K. Schiemann, and D. Waalboer designed and synthesized all new compounds; P.C. and D.M. analyzed crystallographic data; D.S. performed SPR experiments; G.B., W.C., K.E., E.F., S.G., O.A.-P., O.P., R.T.P., M.-J.O.-R., M.S. and R.S.S. developed and performed cell-based assays; K.E., A.d.H.B. and M.V. performed *in vivo* studies. A.B., P.A.C., T.D., C.E., S.A.E., A.M., F. Rohdich, F. Raynaud, K. Schiemann, K. Schneider, R.S., P.W., D. Wienke and J.B. designed studies and analyzed results. J.B., P.A.C., T.D. and D. Wienke wrote the paper.

Competing financial interests

The authors declare competing financial interests: details accompany the online version of the paper.

Additional information

Supplementary information, chemical compound information and chemical probe information is available in the online version of the paper. Reprints and permissions information is available online at http://www.nature.com/reprints/index.html. Correspondence and requests for materials should be addressed to J.B., P.A.C., T.D. or D.W.

ONLINE METHODS

SILAC assay for target identification. Carried out by Evotec AG, Munich, Am Klopferspitz 19a, 82152 Martinsried, Germany[18]. LS174T-L5 cells, a derivative of LS174T cells that have been transduced with a TCF/LEF reporter construct[10] were grown in medium containing either arginine and lysine (Light) or heavier isotopic variants of these amino acids (Medium and Heavy). Proteins captured from the cell lysates by inhibitor-coupled Sepharose beads were eluted, subjected to tryptic digestion and analyzed by quantitative mass spectrometry.

Crystal structure of CDK8–cyclin C in complex with CCT251545 (PDB code 5BNJ). Human CDK8–cyclin C complex was expressed, purified and crystallized as described previously[22,49]. Protein at a concentration of 11.3 mg/ml was crystallized at 20 °C by hanging drop vapor diffusion against 20% PEG 3350 and 0.2 M sodium formate. Crystals were back-soaked and assessed for different time periods within intervals from 5 min up to 24 h within a concentration range of 0.2–2 mM ligand and shock-frozen with 25% ethylene glycol as cryoprotectant. The best crystal used for structure determination belonged to the orthorhombic space group $P2_12_12_1$ with cell constants of $a = 70.78$ Å, $b = 71.49$ Å, $c = 172.54$ Å and $\alpha = \beta = \gamma = 90°$. X-ray diffraction data were collected on X06SA-PX beamline at Swiss Light Source synchrotron radiation source using Pilatus detector and the images were indexed, integrated and scaled using XDS and XSCALE program packages. The structure was solved by molecular replacement using the program MOLREP from the CCP4 program suite with a previous solved model. Subsequently, several cycles of refinement using the program REFMAC and crystallographic model building using the graphic package COOT were applied. Water molecules were built at stereochemically reasonable sites. For crystallographic data and refinement statistics see **Supplementary Table 8**, for an $F_o – F_c$ omit map at 2.5σ cutoff see **Supplementary Figure 17**.

CDK8–cyclin C and CDK19–cyclin C reporter displacement assay. Binding kinetics were determined using a reporter displacement assay. In brief, the assay is based upon the competitive displacement of a reporter probe designed to selectively target the ATP binding site of CDK8 or CDK19 with a fast binding kinetic signature. Binding of the probe to its target results in the emission of an optical signal. Competitive displacement of the probe by the corresponding compounds results in a loss of the optical signal that can be quantified with increasing compound concentrations. IC_{50} values and kinetic parameters of the tested inhibitors were determined as described previously[51].

Protein expression and purification. CDK8–cyclin C complex was purchased from Proteros Biostructures. Human CDK8(1–464) and human cyclin C(1–283) were separately expressed in insect cells and purified by affinity and size exclusion chromatography (SEC). The complex was formed *in vitro* and further purified by SEC. A tool compound which binds to the CDK8 ATP-site, was added to stabilize the complex upon proteolytic removal of the GST fusion tag. In the final purified complex cyclin C is fused to an S-tag.

SPR protocol. CDK8–cyclin C protein complex was immobilized onto CM5 (series S) sensor chips using standard amine coupling. HBS-N, which consisted of 10 mM Hepes pH 7.4, 0.15 M NaCl, was used as a running buffer. The carboxymethyldextran surface within one side of the flow cell was activated with a 7 min injection of a 1:1 ratio of 0.4 M EDC and 0.1 M NHS. CDK8–cyclin C protein complex was diluted in 10 mM BisTris, pH 6.5 with 2µM staurosporine to a concentration of 10 µg/ml. The enzyme was coupled to the surface with a 1- to 3-min injection at a flow rate of 10 µl/min. Remaining activated groups were blocked with a 7 min injection of 1.0 M ethanolamine, pH 8.5. Typically 3,000 ± 1,000 RU of CDK8–cyclin C protein complex was immobilized. Compounds (stored as 10 mM stock solutions in 100% dimethyl sulfoxide (DMSO)) were dissolved directly in running buffer (20 mM HEPES, pH 7.4, 150 mM NaCl, 5 mM MgCl₂, 1 mM DTT, 0.05% P20, 0.1 mM EGTA, 2% DMSO) and analyzed with a Biacore S51 using a twofold dilution series. The highest compound concentration varied according to the expected dissociation constant and all compounds were tested at 10 different concentrations, each concentration was tested at least three times. Interaction analysis cycles consisted of a 120 s sample injection (30 µl/min) followed by 350 s of buffer flow (dissociation phase). All sensorgrams were processed by first subtracting the binding response recorded from the control surface (reference spot), followed by subtracting an average of the buffer blank injections from the reaction spot. To determine kinetic rate constants, all data sets were fitted to a simple 1:1 interaction model including a term for mass transport using numerical integration and nonlinear curve fitting. Equilibrium analysis was performed by fitting the response at the end of the association phase to a single-site binding isotherm.

Cell and organoid culture. All cells used in this study were obtained from ATCC (LGC Promochem), were confirmed to be mycoplasma free using a Mycoplasma detection kit (Lonza, LT017-710) and were authenticated by short tandem repeat profiling. Cells were propagated at 37 °C in a humidified incubator with 5% CO₂ in air using Dulbecco's Modified Eagle's Medium without phenol red (Gibco #41966) and supplemented with 10% (v/v) fetal bovine serum (Biosera cat. #F1830), 2% (v/v) L-glutamine (GIBCO cat. #25030) and 1% (v/v) non-essential amino acids (GIBCO cat. #11146) and sub-cultured when they reached 80% confluence. Tet-O–β-catenin intestinal organoid culture and RNA extraction was carried out as previously described[29].

CETSA (cellular thermal shift assay) analysis. SW620 cells were incubated for 2 h with indicated concentrations (30, 3, 0.3, 0.03 and 0.003 µM) of compound 1, sorafenib, linifanib or ponatinib. Control cells were treated with 0.3% DMSO. Cells were lysed in lysis buffer (50 mM Tris-HCl pH 7.4, 150 mM NaCl, 1% Triton X-100, 1 mM EDTA, 20 mM β-Glycerolphosphate, 1% Phosphatase-Inhibitor Cocktail Set II (Calbiochem, Cat. #524625), 0.1% Protease-Inhibitor Cocktail Set III (Calbiochem, Cat. #539134), 0.01% Benzonase (Novagen, Cat. #70664)) and each lysate was split into two aliquots. One aliquot was kept at 4 °C and the other aliquot was heated at 50 °C for 3 min followed by cooling at room temperature for 3 min. After centrifugation (4 °C, 16,000 × g, 20 min) CDK8 and CDK19 levels were determined in supernatants using a bead-based ELISA.

Immunoblotting analysis of protein expression. Cells (2 ml) were plated into 6-well plates at a density of 1×10^5 cells/ml and were incubated in a humidified tissue culture incubator for 24 h at 37 °C and 5% CO₂. DMSO-dissolved test compounds were added to the wells at specific concentrations and incubated for 6 h, after which cells were lysed with RIPA buffer on ice, frozen at −80 °C overnight and probe-sonicated for complete extraction of nuclear and cytoplasmic proteins. The lysates were centrifuged at 13,000 rpm for 15 min and proteins harvested in the supernatant and protein concentration measured using the BCA assay. 20 µg of protein was added to 2 × loading buffer and boiled for 5 min at 95 °C. Samples were resolved on SDS-4–12%PAGE gels. After transfer to nitrocellulose membranes, blots were blocked at room temperature for 1 h in 5% BSA in TBS-T (0.1% Tween 20, 50 mM Tris-Cl, pH 7.6, 150 mM NaCl) and incubated at 4 °C overnight with antibodies specific for phospho-STAT1^SER727 (Cell Signaling, #8826), total STAT1 (Santa-Cruz, #346), GAPDH (Merck Millipore, MAB374), Phospho-POLR2A^SER2 (#A300-654A), Phospho-POLR2A^SER5 (Bethyl Labs, #A300-655A) or total POLR2A (Bethyl Labs, #A300-653A). After washing with TBS-T, blots were incubated with HRP-conjugated secondary antibodies in blocking buffer at room temperature and bands were visualized using the enhanced chemoluminescence (ECL prime) method. Uncropped immunoblots for **Supplementary Figures 10, 11** and **15** can be found in **Supplementary Figure 18**.

Generation of monoclonal rabbit antibodies against phospho-E2F1^SER375. A monoclonal rabbit antibody against phospho-E2F1^SER375 was generated by Epitomics, Inc. Briefly, rabbits were immunized with 5 boosts of the peptide NH2-RAPVDEDRL(pS)PLVAADSC conjugated to KLH. Antibody titer was monitored by ELISA using the same phosphopeptide used for the immunization but conjugated to BSA. In addition, a phosphopeptide corresponding to the equivalent region in murine E2F1 (RVPMEEDQL(pS)PLVAADSC) and the unphosphorylated peptide of the human protein (RAPVDEDRLSPLVAADSC) were used for screening. Following the selection of the rabbit with the best signal in the ELISA, lymphocytes were isolated from its spleen und fusion was performed to obtain hybridomas. Multiclone hybridoma supernatants were screened by ELISA as above and hybridomas with the desired profile were further subcloned and re-screened to identify the final hybridoma clone. The cDNAs from the IgG heavy chain and light chain were amplified by PCR, sequenced, inserted into a mammalian expression vector and transiently expressed in HEK293 cells. Recombinant antibody was purified using a protein A column and then used in a bead-based ELISA together with commercially available antibodies against total E2F1 (sheep-anti-E2F-1, R&D Systems #AF4825 and rabbit-anti-E2F-1, Cell Signaling #3742) to quantify phospho-E2F1^SER375 and total E2F1. **Supplementary Figure 10** shows the final validation of the total-E2F1 and phospho-E2F1^SER375 reagents in cells co-expressing an inducible CDK8 and E2F1^WT or mutant E2F1^S375A/E2F1^S375D.

shRNA protocol. The human colon cancer cell line Colo205 was transduced with a lentivirus encoding a short half-life luciferase (with a destabilized PEST sequence construct; construct F1921): 16× TCF/LEF transcription sites–short-half-life firefly luciferase on a basal pTA promoter–hygromycin resistance gene on an EF-1-α promoter. This construct was made in-house using the lentiviral base vector: pCDH-CMV-MCS-EF1-Hygro from System Biosciences (cat. #CD515B-1). This generated the Colo205-F1921 subline expressing a luciferase with a half-life of about 60 min.

TRIPZ and GIPZ shRNA gene knockdown constructs for CDK8 (V2THS_112900, V2THS_112909, V2THS_112911) and CDK19 (V2LHS_77136, V3LHS_356652, V2LHS_202355) were purchased from Open Biosystems (GE Healthcare Dharmacon Inc) as bacterial glycerol stocks and plasmid DNA was extracted from an overnight culture using a Qiagen MiniPrep kit. Viral supernatant was produced by co-transfection of individual constructs with packaging plasmids into HEK293 cells and incubation for 48 h. The spun supernatant was tested for optimal titer with Lenti-X GoStix (Clontech Takara Bio). A supernatant cocktail that contained either all three CDK19 or CDK8 packaged constructs was used to spinnoculate sub confluent Colo205-F1921 cells and seeded into 6 well plates with the addition of Polybrene at 8 μg/ml. After 48 h cells were trypsinized and reseeded into 175-cm³ tissue culture flasks containing 1 μg/ml puromycin to select stable clones. After antibiotic selection for one week, the transduced Colo205-F1921 cells were FACS sorted for either GFP-positive, RFP-positive or GFP+RFP-positive cells and expanded in culture. For analysis of TCF-dependent transcriptional activity, 100 μl of cells were plated into 96-well plates (Corning 3917) at a density of 2×10^5 cells/ml and cultured for 24 h as described above. Cells were then lysed using 100 μl of Steady-Glo luciferase reagent (Promega, E2520) and luminescence read on a TopCount luminometer (Perkin Elmer) after 60 min incubation at ambient temperature in a semi-dark room.

esiRNA protocol. Pools of esiRNA targeted against CDK8, CDK19, β-catenin, APC and Renilla luciferase (control) mRNA were obtained from Sigma (cat. #EHU023981, EHU061571, EHU139421, EHU079171 and EHUFLUC respectively). 10.0 ng of each esiRNA pool were pipetted into single wells of a white 384 well plate (Greiner M1437-32EA) and made up to 20 ng total per well if necessary with control esiRNA in a total volume of 5 μl in water. To this was added 0.28 μl/well Hiperfect siRNA transfection reagent (Qiagen 301705) made up to a total volume of 7 μl/well with OptiMEM (Invitrogen 31985-047). After complex formation (10 min), 6000 7dF3 WNT reporter cells[11] in 30 μl medium was pipetted into each well. After 24 h of incubation at 37 °C/5% CO₂, 5 μl of 40 μM estradiol (Sigma E2257) in medium (diluted from a 2 mM stock in ethanol) was added to activate the Dvl2-ER fusion protein and induce WNT pathway activity. After a further 24 h incubation, 50 μl BrightGLO luciferase substrate reagent (Promega E2620) was added to each well for 5 min. The resulting luminescence was then quantified on a Fluostar plate reader (BMG) in luminescence mode. The experiment was repeated 3 times.

CDK8 overexpression. Constructs coding for mycCDK8wt and its kinase-dead (D173A) mutant were inserted into the FRT site of previously described T-Rex HEK293 Tet-O cells (Life Technologies) that have the TCF-firefly luciferase-IRES-GFP (TLIG) reporter[10]. The cells were maintained in culture in DMEM with high glucose supplemented with GlutaMAX, Pen/Strep, 12 μg/ml Blasticidin and 300 μg/ml Hygromycin (Life Technologies). For the luciferase assay, cells were seeded at 30,000 cells/well into a 96-well plate in 80 μL medium. 24 h later, the cells were treated with 0.05 μg/ml doxycycline in H₂O or H₂O alone (4 wells per treatment). After 6 h, the medium was removed and the cells were lysed in 50 μL/well Glo lysis buffer (Promega) with agitation for 5 min. 50 μL Bright Glo reagent (Promega) was then added to each well and the luciferase intensities were read using a BMG FLUOstar Optima plate reader in luminescence mode. For the Western Blot, cells were seeded at 900,000 cells per well of a 6-well dish in 2 ml medium and treated as shown above, at the same time. Cells were harvested in RIPA buffer, separated by SDS gel electrophoresis and probed with antibodies to CDK8 and β-tubulin (Cell Signaling 4196S and 2146S respectively). The experiment was repeated 4 times.

qRT-PCR. RT reactions were carried out on 300–1,000 ng RNA with the Improm II kit (Promega) according to the manufacturer's instructions. The PCR reactions were performed in the Sensimix Sybr green 2× mastermix (Bioline) on an Opticon Chromo II qPCR machine using 40 cycles of 95 °C for 15 s, 55 °C for 15 s and 72 °C for 15 s. Relative expression values were calculated using the $\Delta\Delta C_T$ method[52]. The significance was determined with Kruskal-Wallis non-parametric ANOVA and Dunn's *post hoc* tests. Details of primers used for qRT-PCR can be found in **Supplementary Table 12**.

Tet-O-Δ1-89–β-catenin mouse studies. Cohorts of eight randomly allocated mice were used for each treatment. The drinking water was supplemented with 2 mg/ml doxycycline (Sigma) and 10 mg/ml sucrose for 6–9 days to induce the hyperplastic small-intestine crypt phenotype. Doxycyline was withdrawn for the 'Dox Removal' cohort but was continued for the remainder. In addition, it was necessary to supplement this with an intraperitoneal injection (i.p.) of 2 mg/ml doxycycline in PBS (1% w/v) to maintain levels. The latter was given concurrently with vehicle alone (10% DMSO/5% Tween 20/85% 0.9% NaCl) or vehicle + 100 mg/kg **2** given 3 times over 24 h by oral gavage. RNA extraction was carried out from 3 mm sections of the anterior duodenum (stored in RNAlater (Sigma) at 4 °C overnight) as previously described[34]. qRT-PCR was performed as described above. For dose-dependent experiments, 18.75, 37.5 and 75 mg/kg **1**, **6** or vehicle was orally gavaged twice a day for 2 days as above and BrdU (Sigma) at 2 mg/ml in PBS was injected i.p. 2 h before euthanasia.

Gene-expression microarray. Total RNA was also analyzed by microarray expression profiling. Organoid or cell line total RNA was labeled with Cye3-CTP and a mouse or human reference standard RNA (Stratagene) was labeled with Cye5-CTP by direct incorporation using a Quick-Amp labeling kit (Agilent). Purified, labeled cDNA products were hybridized to 8 × 60K mouse or human microarray following the manufacturers' instructions (Agilent). Microarray slides were washed, scanned and analyzed. Mouse organoid data were analyzed using Arraytools (http://linus.nci.nih.gov/BRB-ArrayTools.html) and the colon cancer cell line data using Genespring (Agilent). A similar analysis was performed on both data sets. Lowess intensity dependent normalization was used to adjust for differences in labeling intensities of the Cy3 and Cy5 dyes[53]. We identified genes that were differentially expressed using a multivariate permutation test to provide confidence that the false discovery rate was less than 5% (refs. 53,54). The test statistics used were random variance *t*-statistics for each gene[53]. Although *t*-statistics were used, the multivariate permutation test was non-parametric and does not require the assumption of Gaussian distributions. The significantly differentially expressed genes were investigated for enrichment in terms of particular pathways or potential transcription factor regulation using the Metacore software (Thomson Reuters). Microarray data are available on the NCBI Gene Expression Omnibus (GEO; http://www.ncbi.nlm.nih.gov/geo/) website under accession number GEO GSE67849.

Effect on crypt morphology by immunohistochemical staining. Duodenal segments from treated mice were fixed overnight in 10% (v/v) formaldehyde in PBS for 16 h at 4 °C, embedded in paraffin by standard automated techniques and sectioned. Sections were deparaffinized in 3 changes of xylene and rehydrated through graded alcohols (2× 100%, 2× 95%, 1× 70% ethanol (v/v) in water). Subsequently, they were placed in 2 N HCl for 30 min at 37 °C, rinsed thoroughly in PBS and then treated for a further 20 min at 37 °C with 100 μl pre-warmed 0.05% trypsin in PBS (Invitrogen). The sections were then rinsed with PBS and blocked in 100 μl blocking solution from the Mouse-On-Mouse immunostaining kit (Vector Labs) for 1 h, followed by incubation with 1:1,000 anti-BrdU mouse monoclonal antibody (clone BU-33, Sigma B8434) in MOM solution (from the Mouse-on-Mouse immunostaining kit from Vector Labs) overnight at 4 °C. This was followed by treatment with the biotinylated secondary antibody and ABC solution from the Mouse-On-Mouse immunostaining kit (Vector Labs) according to the manufacturer's instructions. The sections were counterstained with Mayer's hematoxylin (Sigma) for 1 min, copiously washed in tap water and dehydrated though graded alcohols (1× 70%, 2× 95%, 2× 100% ethanol (v/v) in water) and 3 changes of xylene. The sections were then mounted in DPX (Sigma). Sections for Alcian Blue staining to detect the goblet cells were processed according to the method previously described[55]. Crypt length, % BrdU positive cells and % goblet cells were counted in 50 crypts according to the half-crypt scoring system previously described[56]. The Kruskal-Wallis non-parametric ANOVA with Dunn's *post hoc* tests was used to determine the significance of the results.

MMTV-WNT-1 allograft transplant model. MMTV-WNT-1 allograft tissue from immuno-compromised mice[40] was chopped into fragments of <1 mm³ and transplanted using a trochar into the flanks of CD1(*nu/nu*) mice that had been transiently anaesthetized with isofluorane. Once the tumors had grown to >5mm³,

the animals were randomly assigned to three cohorts of 8 to be orally gavaged with vehicle (10% DMSO/5% Tween 20/85% 0.9% NaCl), 37.5 mg/kg or 75 mg/kg **1**, twice a day for 10 days. Tumor dimensions were measured daily using a caliper. Tumor volume in mm^3 was calculated using the formula: volume = (width^2 × length)/2. Tumor tissue samples for RNA extraction were stored in RNAlater (Sigma) at 4 °C overnight and RNA isolation was carried out as previously described[29].

SW620 3D clonogenic assay. The assay was performed in 96 well format according to a modified two-layer soft agar assay[57]. Each test well contained three layers of equal volume: 2 layers of semi-solid medium (bottom and top layer), and one layer of medium supernatant, with or without test compound. The bottom layer consisted of 0.1 ml/well MEM Alpha Medium (supplemented with 10% (v/v) FCS, sodium bicarbonate, penicillin-streptomycin (Pen Strep), L-glutamine, sodium pyruvate and 1% (w/v) agar). 4×10^3 cells were added to 0.1 ml of the same culture medium supplemented with 0.7% (w/v) agar and plated in onto the bottom layer. Compound **1** was added after serial dilution in DMSO and transfer in cell culture medium, and left on the cells for the duration of the experiment (continuous exposure, 0.03 ml drug overlay). Each plate included six untreated control wells and drug treated groups in quadruplicate at 15 concentrations (compound concentration range from 30 μM to 10 pM). Cultures were incubated at 37 °C and 10% CO$_2$ in a humidified atmosphere for 14 days. Viability of tumor cells in soft-agar culture was determined by Alamar Blue staining. The full dose-response curve from four technical repeats is shown in **Supplementary Figure 15**.

SW620 human tumor xenograft model. Three million SW620 human colorectal carcinoma cells were injected s.c. in the right flanks of female NCr athymic mice 6–8 weeks of age. Therapy was initiated when established tumors reached a mean volume of 60 mm (day 13). Animals were randomly assigned to two cohorts of 10. Control mice received vehicle (10% DMSO, 5% Tween 20, 85% saline) and treated animals compound **1** at 70 mg/kg orally twice a day with a 2-day break after 1 week's dosing. Tumor volumes and body weights were measured three times weekly and the study was terminated on day 14. Plasma and tumor samples were collected for pharmacokinetic and pharmacodynamic biomarker analysis.

Pharmacokinetic analysis. Plasma and tumor homogenates were extracted with 3 equivalent volumes of methanol containing olomoucine (500 nM) as an internal standard. Extracts were quantified for compound **1** using an external calibration method (8 point calibration curve with 4 quality control samples) by multiple reaction monitoring on an Agilent 6410 triple quadrupole mass spectrometer following chromatographic separation using a Phenomenex Kinetex C 18 HPLC column (2.6 μm, 50 mm × 2.1 mm ID) with a 5 min linear gradient 90/10 to 10/90 0.1% formic acid/methanol on an Agilent 1290 LC system.

Phospho-STAT1^{SER727} protocol. Tumors were excised, immediately snap-frozen in liquid nitrogen and stored at −80 °C. Samples were later transferred to MK28 reinforced homogenizing tubes with metal beads (Stretton Scientific) lysis buffer and phosphatase inhibitors (Sigma P5726 and P0044 1:50 dilution) added immediately. The samples were ground using a Precellys 24 at 6,000 rpm, 2 × 20 sec (Stretton Scientific). Tumor lysates were frozen at −80 °C, thawed, sonicated in a water bath for 3 min, then incubated on ice for 10 min. Tubes were spun at 14000 rpm at 4 °C for 10 min and supernatants were collected, aliquoted and frozen at −80 °C until analysis. Tumor lysates were diluted 1:5 in lysis buffer and the concentrations determined using a Direct Detect spectrometer (Merck Millipore). Samples were aliquoted, then boiled in electrophoresis sample buffer and loaded on SDS/4–12% PAGE gels. After transfer to PVDF membranes, blots were blocked at room temperature for 1 h in blocking buffer (5% dry milk in TNT: 1 M Tris HCl, pH8, 5 M NaCl, 0.1% Tween 20) and incubated at 4 °C overnight with 1:1,000 rabbit anti-STAT1 (Santa Cruz, sc-346), 1:2,000 rabbit anti p-STAT1^{SER727} (Cell Signaling Technology, #8826) or 1:10,000 mouse anti-GAPDH (Abcam, Ab-8245) antibodies. After washing with TNT, blots were incubated with HRP-conjugated secondary antibodies in blocking buffer at room temperature and bands were visualized using the enhanced chemoluminescence (ECL prime) method.

All animal studies were conducted in accordance with guidelines for the welfare and use of animals in cancer research[58]. We comply with the UK National Cancer Research Institute Guidelines and all work is approved by our own institutional Ethics Committee and the UK Government's Home Office.

51. Neumann, L., von Konig, K. & Ullmann, D. HTS reporter displacement assay for fragment screening and fragment evolution toward leads with optimized binding kinetics, binding selectivity, and thermodynamic signature. *Methods Enzymol.* **493**, 299–320 (2011).
52. Livak, K.J. & Schmittgen, T.D. Analysis of relative gene expression data using real-time quantitative PCR and the $2^{-\Delta\Delta C(T)}$ method. *Methods* **25**, 402–408 (2001).
53. Simon, R. *et al. Design and Analysis of DNA Microarray Investigations* (Springer, New York, 2003).
54. Korn, E.L. *et al.* Controlling the number of false discoveries: application to high-dimensional genomic data. *J. Stat. Plan. Inference* **75**, 447–460 (2012).
55. Sansom, O.J. *et al.* Loss of Apc in vivo immediately perturbs Wnt signaling, differentiation, and migration. *Genes Dev.* **18**, 1385–1390 (2004).
56. Li, Y.Q. *et al.* Target cells for the cytotoxic effects of carcinogens in the murine small intestine. *Carcinogenesis* **13**, 361–368 (1992).
57. Hamburger, A.W. & Salmon, S.E. Primary bioassay of human tumor stem cells. *Science* **197**, 461–463 (1977).
58. Workman, P. *et al.* Guidelines for the welfare and use of animals in cancer research. *Br. J. Cancer* **102**, 1555–1577 (2010).